

## Article

# Kinetic and Thermodynamic Analyses of Co-Pyrolysis of Nylon-Polyethylene Pouch Wastes

Hai-Bo Wan and Zhen Huang \* 

Tianjin University of Commerce, Tianjin 300134, China; wanhaibo@tjcu.edu.cn

\* Correspondence: huangzhen@tjcu.edu.cn; Tel.: +86-22-2668-6264; Fax: +86-22-2668-6251

**Abstract:** In this study, thermogravimetric measurements of nylon-6/polyethylene double-layer pouch wastes were conducted in N<sub>2</sub> under a constant heating-rate mode, and the multiple heating-rate results were analyzed in terms of degradation features and specific temperatures. Experimental results show that the waste pyrolysis involves one reaction stage, and all specific parameters appear to increase with the heating rate. Kinetic analysis of non-isothermal data was thoroughly performed using various isoconversional model-free methods for the calculations of the activation energy, resulting in 143~215 kJ/mol over the whole pyrolysis process. By means of the model-fitting method, the reaction mechanism model  $g(\alpha)$  and pre-exponential factor  $\ln k_0$  are concurrently determined with the aid of the linear compensation effect. With such methodology proposed, the Avrami-Erofeev kinetic model  $A_{3/2}$  of  $g(\alpha) = [-\ln(1 - \alpha)]^{2/3}$  is found to be the most appropriate mechanism function for describing the pyrolysis of the nylon-6/polyethylene waste along with  $\ln k_0$  of 23.14 to 34.26 min<sup>-1</sup>. With the Arrhenius parameters thus obtained, the predictions were made and performed very satisfactorily to correlate experimental results. Additionally, the service life and thermodynamic parameters over the entire pyrolysis process were also estimated.

**Keywords:** plastic wastes; co-pyrolysis; thermogravimetric analysis; isoconversional kinetics



**Citation:** Wan, H.-B.; Huang, Z. Kinetic and Thermodynamic Analyses of Co-Pyrolysis of Nylon-Polyethylene Pouch Wastes. *Materials* **2023**, *16*, 5738. <https://doi.org/10.3390/ma16175738>

Academic Editors: Giovanni Pappalettera and Sanichiro Yoshida

Received: 5 July 2023

Revised: 12 August 2023

Accepted: 18 August 2023

Published: 22 August 2023



**Copyright:** © 2023 by the authors. Licensee MDPI, Basel, Switzerland. This article is an open access article distributed under the terms and conditions of the Creative Commons Attribution (CC BY) license (<https://creativecommons.org/licenses/by/4.0/>).

## 1. Introduction

Today, plastic films are widely applied in the food packaging industry such as various flexible packaging articles, liners inside cartons and lidding on cups. In these usages, plastic films can be employed alone or in combinations to serve as diverse packages for various fresh produce. Thus, these films should satisfy the industry requirements and consumer desires so as to maintain food safety and minimize environmental damage. Therefore, polymers used to make packaging plastic films are required to balance the packaging permeability requirements, the respiratory activities of the fresh foods and the surrounding temperature and humidity. Among these plastic films used, nylon-6/polyethylene (N-PE) double-layer films appear very attractive for preserving fresh foods [1,2] since their mechanical, thermal and gas-permeable properties complement each other [3]. With the rapid development of the food packaging industry and the demand for plastics, the accumulation of plastic waste has increased, and the environmental hazards thus caused have gained widespread concern around the world. Among various plastic waste disposal technologies, pyrolysis appears to be notable because it can recover value-added chemical species from plastic wastes and efficiently minimize environmental risks [4].

For the purpose of studying pyrolysis processes, thermogravimetric analysis (TGA) is known to be the most widely used method [5–7]. Along with experimental attempts, theoretical kinetic analysis of the plastic pyrolysis process has also played a vital role in guiding the pyrolysis reactor design and providing theoretical support for industrial application. Based on TGA data over different heating rates, model-free and model-fitting methods are two parallel ways for performing kinetic pyrolysis analysis in terms of kinetic triplet parameters of apparent activation energy  $E_k$ , pre-exponential factor  $k_0$  and reaction

mechanism model function  $f(\alpha)$  [8–10]. By means of the model-free method, the activation energy can be more reliably resulted because there is no involvement of any pyrolysis mechanism assumption. In contrast, model-fitting methods can be attempted for obtaining both the pre-exponential factor and the pyrolysis reaction mechanism function. Usually, the study of pyrolysis behavior and kinetic analysis has been performed on individual plastics since it aids to comprehend the pyrolysis of plastic blends [5,6].

In the current study, nylon-6/polyethylene (N-PE) double-layer film pouch wastes were collected locally in Tianjin, China, for inert pyrolysis decomposition considerations. Up to now, many efforts have been made to individually investigate the pyrolysis of nylon-6 [11–14] and polyethylene [15–18] so as to provide necessary knowledge for thermochemically converting their wastes into valuable chemical compounds for sustainable energy recovery. These kinetic works have shown that for the pyrolysis of nylon-6 [11–14], it has  $E_k = 113\sim 266$  kJ/mol and  $\ln k_0 = 8.7\sim 15.0$  min<sup>-1</sup> while its one-step decomposition may be controlled by the order-based chemical reaction Fn model of  $n = 0.33\sim 1.9$ . As for the pyrolysis of PE [15–18], the  $E_k$  and  $\ln k_0$  values are found to vary between 135 and 250 kJ/mol, or  $3.32 \times 10^{17}\sim 2.20 \times 10^{21}$  min<sup>-1</sup>, respectively, while the one-step pyrolysis appears to be also controlled by the order-based chemical reaction models of the  $F_{1/2}$  model with  $g(\alpha) = 1 - (1 - \alpha)^{1/2}$  or the F1 model with  $g(\alpha) = -\ln(1 - \alpha)$ . However, Budrugaec et al. [7] proposed a very complex LDPE pyrolysis composed of four successive stages: Avrami–Erofeev kinetic models (An), reaction order (Fn), reaction order (Fn), and three-dimensional diffusion (D3). Obviously, these kinetic parameters are different from diverse works and somewhat disagreeable with each other. The main reason for it may be related to the different sources of raw samples, different preparation techniques and the introduction of fillers, experimental programs and instrument limitation conditions [7].

The main contributions of the present work are as follows: (1) Pyrolysis features and kinetics of N-PE waste in inert nitrogen were fully obtained by using a thermogravimetric analyzer. To our best knowledge, there is no report on the pyrolysis investigation of the nylon-6 and PE mixture, and such work is required not only to get information about pyrolysis features and kinetic parameters over the whole temperature range but also to provide pyrolysis process predictions necessary for thermochemically processing massive N-PE waste. (2) Non-isothermal mass loss data were kinetically analyzed to determine the activation energy with various model-free methods, and the calculation results with these methods were compared. (3) A new compensation-effect-aided model-fitting method was attempted to determine the most appropriate mechanism function for describing the pyrolysis process of N-PE waste and the pre-exponential factor as well. (4) With the kinetic quantities, the predications against experimental mass loss results along with the lifetime estimation were thus made. In addition, thermodynamic parameters were also computed over the entire pyrolysis process according to the transition state theory. The present work provides information about pyrolysis behaviors and kinetic parameters necessary for designing any chemical reactor to thermally dispose of N-PE waste.

## 2. Materials and Analysis Methods

### 2.1. Materials

Nylon-6/PE (N-PE) double-layer pouch wastes, after we completed the preservation packaging test for mango fruits in our laboratory, were collected and washed using distilled water. The double-layer film to make the pouches was determined to have a thickness of about 80  $\mu\text{m}$ , and it was purchased from Cangzhou Senyu Plastics Co., Ltd., Cangzhou, China, and co-extruded with nylon-6 and low-density polyethylene at a mass ratio of 1 to 3. The washed pouch waste samples, after drying at 350 K in a controlled oven for 2 h, were ground mechanically and meshed into powders of less than 100  $\mu\text{m}$  in size for subsequent experiments.

## 2.2. TGA Analysis

A Shimadzu DTG-60 thermogravimetric analyzer was used to carry out thermal degradation measurements and simultaneous differential thermal analysis (DTA) under 30 cm<sup>3</sup> N<sub>2</sub> flow per minute. For all measurements, the N-PE waste samples were weighed to have approximately similar mass of 3~4 mg and then were subjected to heating with a temperature rise of 5, 10, 15 and 20 K per minute from ambient to 850 K. The non-isothermal mass loss data and the first derivative data of thermogravimetric curves (DTG) along with DTA data were all automatically generated and recorded via the accompanied software.

## 2.3. Theoretical Basis for Kinetic Analysis

To deeply understand pyrolysis behaviors of solid materials, kinetic analysis of thermal degradation processes is usually performed, resulting in kinetic triplets in terms of the activation energy ( $E_k$ ), the pre-exponential factor ( $k_0$ ) and the reaction mechanism function ( $f(\alpha)$ ) [8–10]. Theoretically, kinetic triplet parameters can be obtained by using model-free and model-fitting methods to evaluate isothermal pyrolysis data.

In general, pyrolysis process of plastic wastes may be mathematically expressed by the rate of degradation ( $d\alpha/dt$ ) depending on degradation time and temperature:

$$d\alpha/dt = k(T) \cdot f(\alpha) \quad (1)$$

where  $\alpha$  is the degree of pyrolysis degradation defined as  $\alpha = (w_0 - w_t)/(w_0 - w_f)$ , and  $w_0$ ,  $w_t$  and  $w_f$  are the initial mass, the mass at pyrolysis time  $t$  and final mass of the sample, respectively.  $f(\alpha)$  stands for any specific reaction mechanism model in its differential expression, which is commonly taken as the function of  $\alpha$  only, and the  $\alpha$  data could be readily abstracted from experimental TG results.  $k(T)$  is the rate constant of pyrolysis process and is usually thought to depend on absolute temperature  $T$ (K) following Arrhenius law:

$$k(T) = k_0 \cdot \exp(-E_k/RT) \quad (2)$$

where  $k_0$  is the pre-exponential factor (min<sup>-1</sup>), and  $E_k$  and  $R$  are the activation energy (kJ/mol) and gas constant (8.314 J/mol·K), respectively.

Under non-isothermal conditions with a heating rate (K/min) defined as  $\beta = dT/dt$ , one may easily obtain

$$\frac{d\alpha}{dT} = \frac{k_0}{\beta} \cdot \exp(-E_k/RT) \cdot f(\alpha) \quad (3)$$

After transformation, the following may be deduced:

$$g(\alpha) \equiv \int_0^\alpha \frac{d\alpha}{f(\alpha)} = \frac{k_0}{\beta} \int_0^T \exp\left(-\frac{E_k}{RT}\right) dT \quad (4)$$

where  $g(\alpha)$  is the reaction model in the integral expression and stands for a particular pyrolysis mechanism function  $f(\alpha)$ . One may note that the right-hand side of Equation (4) involves a well-known temperature integral, which cannot be analytically solved but can be resolved to be either numerical solutions or diverse approximate solutions. On the other hand, a number of reaction mechanism models in  $g(\alpha)$  or  $f(\alpha)$  have been proposed and can be referred to elsewhere [19,20].

Therefore, kinetic triplets of  $E_k$ ,  $k_0$  and  $f(\alpha)$  must be achieved for completely depicting any pyrolysis process and providing necessary knowledge for any related practical applications. Usually, the  $E_k$  values can be readily calculated by using model-free methods while the  $f(\alpha)$  may be properly judged by means of the model-fitting methodology. As for a third kinetic parameter  $k_0$ , it may be determined thereafter by considering the compensation effect or fitting against experimental results. In present study, model-free and model-fitting methods were applied for kinetically recounting pyrolysis of N-PE wastes.

### 2.3.1. Determination of $E_a$ Based on Isoconversional Methods

For the determination of the activation energy  $E_k$ , a number of model-free methods have been extensively attempted since they do not consider any specific chemical reaction model but are mostly developed by approximating temperature-integral functions [8–10,21,22]. Up to now, the most commonly used integral methods include Coats–Redfern (CR) [23], Flynn–Wall–Ozawa (FWO) [24,25], Madhusudanan–Krishnan–Nina (MKN) [26] and Starink (SK) [27] methods, and they are mathematically expressed as below:

$$\text{CR method: } \ln\left(\frac{\beta}{T^2}\right) = \ln\left[\frac{k_0 R}{E_k g(\alpha)}\right] - \frac{E_k}{RT}. \quad (5)$$

$$\text{FWO method: } \ln \beta = \ln\left[\frac{0.0048 k_0 E_k}{R g(\alpha)}\right] - 1.0516 \frac{E_k}{RT}. \quad (6)$$

$$\text{MKN method: } \ln\left(\frac{\beta}{T^{1.884318}}\right) = \ln\left[\frac{k_0}{g(\alpha)} \left(\frac{E_k}{R}\right)^{-0.884318}\right] - 1.001928 \frac{E_k}{RT} - 0.389677 \quad (7)$$

$$\text{SK method: } \ln\left(\frac{\beta}{T^{1.92}}\right) = \ln\left[\frac{k_0 R}{g(\alpha)} \left(\frac{E_k}{R}\right)^{-0.92}\right] - 1.0008 \frac{E_k}{RT} - 0.312 \quad (8)$$

Following these isoconversional methods, the left term is linearly drawn against  $1/T$ , and a series of straight plots are obtained for all the  $\alpha$  levels considered. From the resultant slopes, the  $E_k$  may be readily estimated over the entire range. As for the CR method, one may note that it has been initially proposed for kinetically evaluating pyrolysis data based on a single heating rate and later upgraded to analyze multi-heating-rate data. For this reason, the latter is sometimes renamed as model-free Kissinger–Akahira–Sunose (KAS) method [28]. However, in this article, the term of the CR method is preferred for studying co-pyrolysis of N-PE waste.

Considering that these methods are of approximate nature, Gao et al. [29] attempted to introduce two iteration terms to finalize the exact solution to temperature-integral function and then proposed a very good iterative program to obtain more accurate  $E_k$  values than the conventional isoconversional methods. The two equivalent iterative methods thus proposed, respectively corresponding to CR and FWO methods, are mathematically given below and named here it-CR and it-FWO in short:

$$\text{it-CR: } \ln\left(\frac{\beta}{h(x) \cdot T^2}\right) = \ln\left[\frac{k_0 R}{E_k g(\alpha)}\right] - \frac{E_k}{RT} \quad (9)$$

$$h(x) = \frac{x^4 + 18x^3 + 86x^2 + 96x}{x^4 + 20x^3 + 120x^2 + 240x + 120} \quad (10)$$

$$\text{it-FWO: } \ln \frac{\beta}{H(x)} = \ln \frac{0.0048 k_0 E_k}{R g(\alpha)} - 1.0516 \frac{E_k}{RT} \quad (11)$$

$$H(x) = \frac{\exp(-x) \cdot h(x)/x^2}{0.0048 \exp(-1.0516x)} \quad (12)$$

where  $x = E_k/RT$ , and the iteration calculation may be briefly described as follows: (1) First, assuming  $h(x) = 1$  or  $H(x) = 1$ , Equations (9) and (11) are respectively reduced to Equations (5) and (6), and  $\ln(\beta/T^2)$  vs.  $1/T$  and  $\ln \beta$  vs.  $1/T$  can be plotted for each  $\alpha$ , leading to the initial value of  $E_{k1}$  from the correspondent straight lines. Clearly, these values are identical to those from CR or FWO methods, respectively. (2) By applying  $E_{k1}$  to calculate  $h(x)$  and  $H(x)$ , followed by drawing  $\ln[\beta/h(x)T^2] \sim 1/T$  or  $\ln[\beta/H(x)] \sim 1/T$ , a new value of  $E_{k2}$  can be computed from the slopes of resultant straight lines. (3) Then, the calculation should be continued by replacing  $E_{k1}$  with  $E_{k2}$  until  $|E_{ki} - E_{ki-1}| < 0.01$  kJ/mol. (4) Finally, the

latest value of  $E_{ki}$  could be considered as the exact activation energy. Accordingly, the  $E_k$  can thus be yielded over the entire conversion range.

### 2.3.2. Determination of $\ln k_0$ and $f(a)$ Based on Compensation Effect

Pre-exponential factor  $\ln k_0$  is another kinetic parameter, and it can be estimated according to the kinetic compensation effect between  $\ln k_0$  and  $E_k$ . Such effect has been recently addressed and exemplified by Prof. Vyazovkin [30] for obtaining model-free  $\ln k_0$  values provided that relatively accurate  $E_k$  values are available from the model-free methods, and it can be linearly expressed as follows:

$$\ln k_0 = aE_k + b \quad (13)$$

where  $a$  and  $b$  are two characteristic compensation parameters, and then  $\ln k_0$  may be calculated by substituting the calculated  $E_k$  into Equation (13) once  $a$  and  $b$  are both available.

In this work, a new model-fitting method is proposed, according to the compensation effect, to determine  $\ln k_0$  and  $g(a)$  together. For such purpose, the intercept of the final iteration based on the it-CR method,  $I_f$ , for estimating  $E_{ki}$  will be used here. From Equation (9), the following can be obtained:

$$I_f = \ln \left[ \frac{k_0 R}{E_{ki} \cdot g(a)} \right] \quad (14)$$

Obviously,  $\ln k_0$  and  $g(a)$  are both involved in Equation (14), and the following expression may be readily deduced from Equation (13):

$$\ln k_0 = I_f - \ln \left[ \frac{R}{E_{ki} \cdot g(a)} \right] = aE_{ki} + b \quad (15)$$

With a known model  $g(a)$ ,  $I_f$  and  $E_{ki}$  obtained from the iteration, the  $\ln k_0$  values can be estimated from Equation (15). Then drawing  $I_f - \ln\{R/[E_{ki} \cdot g(a)]\}$  against isoconversional  $E_{ki}$  over the entire conversion range may yield a straight line for each  $g(a)$ , and the performances of different  $g(a)$  models will be evaluated by comparing the linear correlation coefficient  $R^2$  values. The model  $g(a)$  with the  $R^2$  value of closest to or equal to 1.0 may be taken as the most appropriate one. At the same time, the two parameters of  $a$  and  $b$  will be also determined, and then the  $\ln k_0$  values can be calculated by substituting  $E_{ki}$  into Equation (13).

### 2.3.3. Determination of Thermodynamic Parameters

Thermodynamic quantities for pyrolysis and oxidative thermal degradation of tennis string nylon-6 waste, including activation energy ( $E_k$ ), the change in entropy ( $\Delta S$ ), the change in enthalpy ( $\Delta H$ ) and the change in Gibbs free energy ( $\Delta G$ ), were calculated based on transition-state theory using the following expressions [31–33]:

$$\Delta S = R \cdot \ln[(k_0 \cdot h_p)/(e \cdot k_B \cdot T)] \quad (16)$$

$$\Delta H = E_k - RT \quad (17)$$

$$\Delta G = \Delta H - T\Delta S \quad (18)$$

where  $e$  is the Neper number (2.7183), and  $h_p$  and  $k_B$  represent Plank constant ( $6.626 \times 10^{-34}$  J/s) and Boltzmann constant ( $1.381 \times 10^{-23}$  J/K), respectively. Herein,  $\ln k_0$  is the pre-exponential factor determined as above, and  $E_k$  is the activation energy from the iteration method.

### 3. Results and Discussion

#### 3.1. FTIR Examination

Figure 1 shows FTIR measurements conducted for N-PE waste, and these spectra can be elaborated as follows. The absorption band peaked at  $3290\text{ cm}^{-1}$  can be attributed to the stretching vibrations of hydrogen-bonded NH groups while the adsorption bands centered at  $3049$ ,  $2894$  and  $2651\text{ cm}^{-1}$  can be assigned to the stretching vibration of the  $-\text{CH}$ ,  $-\text{CH}_2$  and  $-\text{CH}_3$  groups. Meanwhile, the band of  $1620\sim 1660\text{ cm}^{-1}$  can be considered as the stretching vibration of the amide II and CN groups of nylon-6, and the one over  $1520\sim 1560\text{ cm}^{-1}$  can be due to the vibrations of amide I, almost identical to those reported in the literature [34]. Furthermore, the bands around  $1450\sim 1470$  and  $1380\sim 1360\text{ cm}^{-1}$  are respectively attributed to the bending vibrations of the  $-\text{CH}_2$  and  $-\text{CH}_3$  groups while the band around  $710\sim 730\text{ cm}^{-1}$  is probably due to the rocking vibration of the  $-\text{CH}_2$  group [35,36]. The above information tends to suggest there may be no strong interaction between nylon-6 and PE, even though they are co-present in the waste sample.

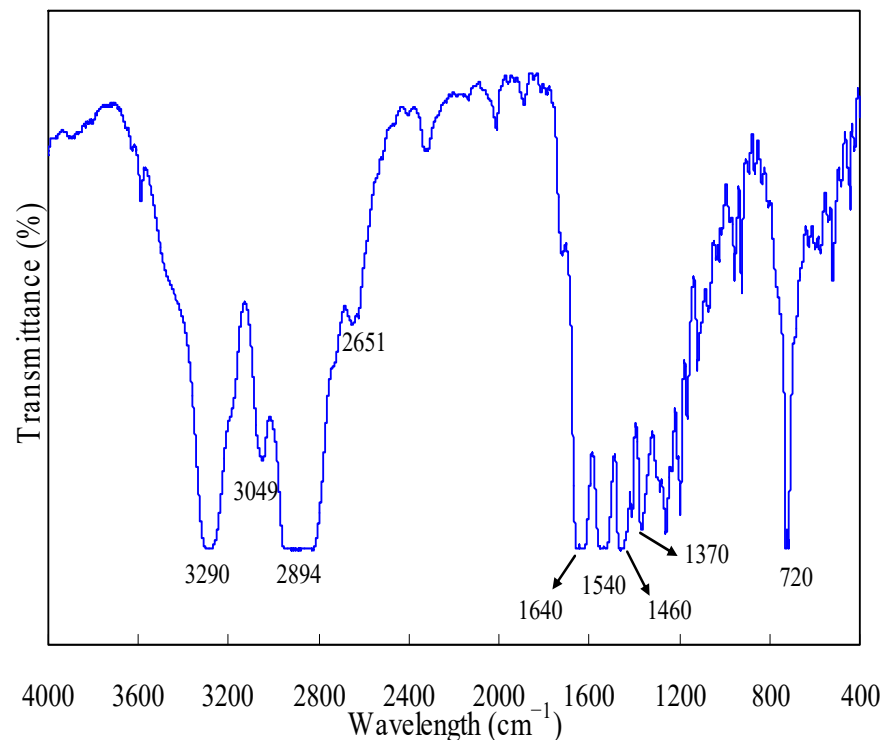


**Figure 1.** FTIR analysis results for N-PE waste.

#### 3.2. Pyrolysis Features of N-PE Waste

Figure 2a graphically presents the TGA results of the N-PE waste sample determined in inert  $\text{N}_2$  under a constant ramping rate of  $\beta = 5, 10, 15$  or  $20\text{ K/min}$ . Clearly as seen, the T-dependent mass loss curve moves to a lower-temperature range as the heating rate  $\beta$  declines and vice versa. For example, the sample is seen to lose its mass in the range of  $629.06\sim 746.24\text{ K}$  at  $5\text{ K/min}$ , but the mass loss range shifts upward to the range of  $652.17\sim 766.85\text{ K}$  at  $15\text{ K/min}$ . Such a result is related to the resistance of the sample to heat transfer. Due to the poor thermal conductivity, the inside and outside of the sample may be evenly heated, and such a case appears to have a worse result as the heating rate goes up. Subsequently, the thermal resistance leads to the nonuniform mass transfer, and some components inside the sample cannot gasify promptly to respond to the rise in the heating rate, instead, leading to a temperature-shift compensation.

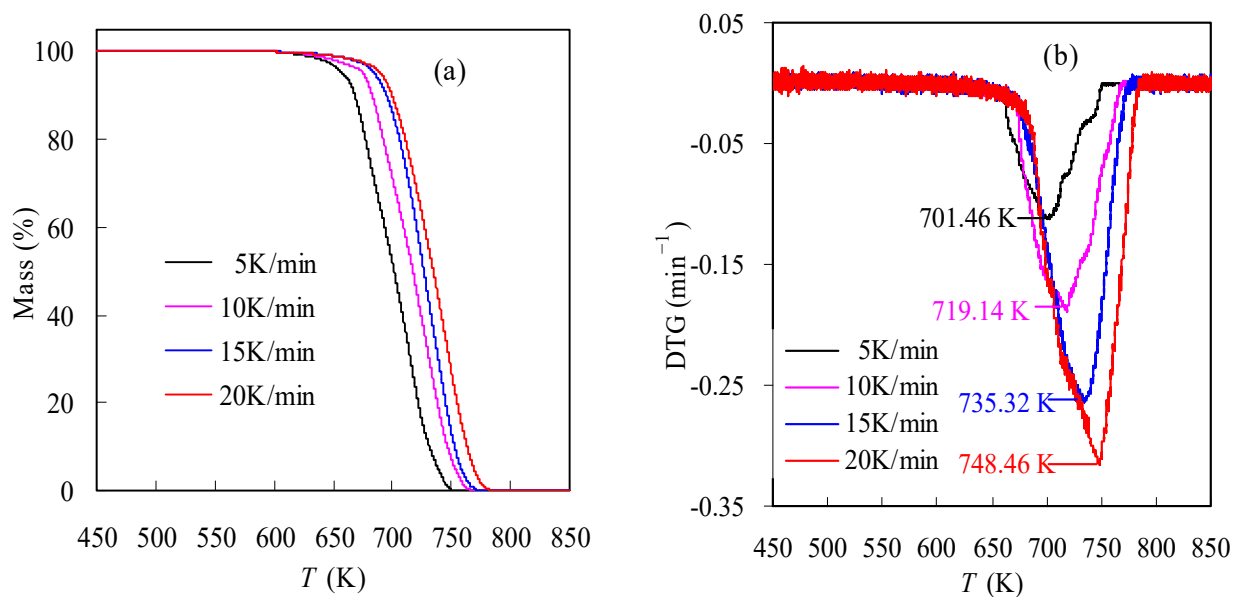


**Figure 2.** Pyrolysis TGA results (a) and DTG curves (b) of the N-PE waste under different heating rates.

Figure 2b reflects the multi-heating-rate DTG curves of the N-PE waste, and one may note that each DTG curve only demonstrates one peak where the sample shows a maximum mass loss rate ( $da/dt$ ). Here, the temperature at the peak is named  $T_p$  for simplicity, resulting in one  $T_p$  for one  $\beta$ . Similar to those observed from the TGA results, the DTG curves are seen to heavily depend on  $\beta$ , and the curve will shift rightward to high-temperature domains as  $\beta$  increases. At the same time, the  $T_p$  value increases, and the peak becomes strong when increasing  $\beta$  from 5 to 20 K/min. More importantly, based on the one-peak features of DTG results, the waste sample may undertake one reaction stage during the pyrolysis process, although two different polymers are involved. Such finding is less frequently reported in publications since two polymers are physically blended by co-extrusion. A possible explanation for it is that the respective pyrolyses of nylon-6 and PE are strongly overlapped with each other, and further effort to confirm this will be made in a subsequent study. Thereafter, a single-reaction model might be assumed for depicting the kinetic degradation process. Such an assumption might be very helpful for obtaining the most appropriate mechanism function for the pyrolysis of N-PE pouch wastes.

To better examine the effect of the heating rate on the mass loss results, some specific temperatures are abstracted from TGA data and redrawn in Figure 3 for the N-PE waste. In Figure 3,  $T_1$ ,  $T_{10}$ ,  $T_{20}$ ,  $T_{90}$  and  $T_{99}$  are specified as the temperatures of 1, 10, 20, 90 and 99% mass conversion, respectively. As clearly seen, the relationship between  $\beta$  and these specific temperatures can be linearly quantified. The linearization parameters and the values of  $R^2$  (defined as the linear correlation coefficient) are all given in Figure 3 for reference. Expectedly, all specific temperatures demonstrate very good linear dependence on the heating rate, indicative of their linear increase with the heating rate used.

On the other hand, the  $\beta$  effect may be also considered by examining thermochemical performances in terms of the heat-resistance index (HRI) [19,37] and comprehensive performance index (CPI) [38,39] with respective mathematical forms as below:

$$HRI = 0.49 \times [T_5 + 0.6(T_{30} - T_5)] \quad (19)$$

$$CPI = \frac{DTG_p \cdot DTG_m}{T_i T_p \Delta T} \quad (20)$$

where  $T_5$  and  $T_{30}$  are, respectively, the temperatures at the mass conversion of 5% and 30% while  $T_i$  represents the temperature at the beginning of pyrolysis.  $DTG_p$  and  $DTG_m$  are

the maximum mass loss rate ( $\text{min}^{-1}$ ) and the average mass loss rate ( $\text{min}^{-1}$ ), respectively. Meanwhile,  $\Delta T$  means the temperature range in-between  $DTG/DTG_p = 0.5$ . Usually, the higher  $CPI$  value suggests a better thermochemical performance.

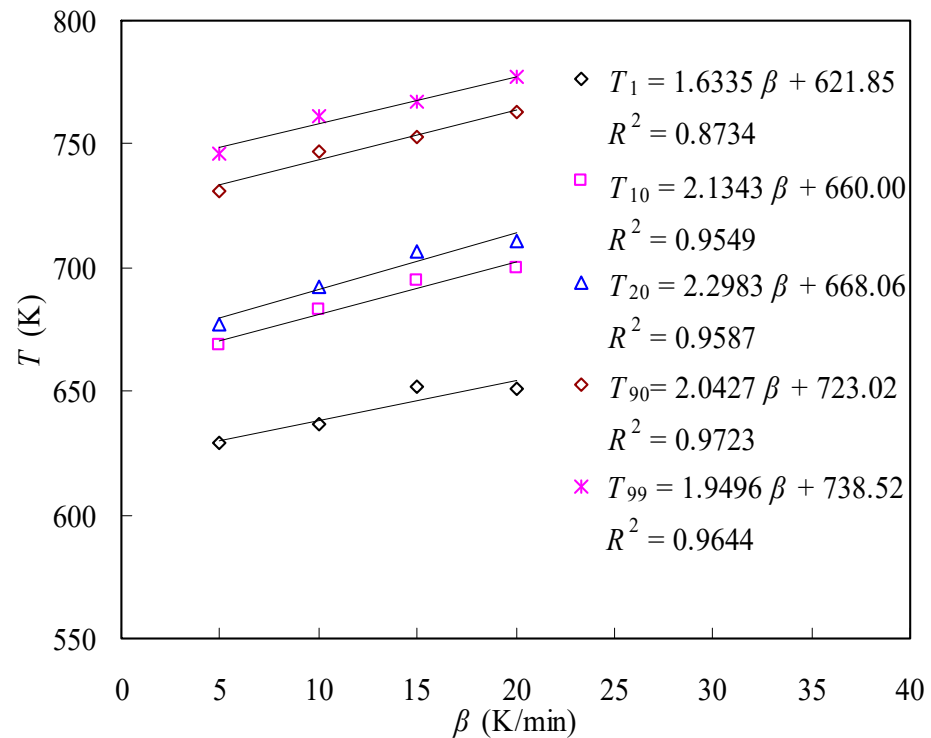


**Figure 3.** Relationship between heating rate  $\beta$  and specific pyrolysis temperatures.

Table 1 presents some featured parameters for the pyrolysis of the N-PE waste. Based on  $T_5$  and  $T_{30}$  from TGA results, the  $HRI$  value can be evaluated according to Equation (2), and it is seen to slightly increase upward as  $\beta$  goes up, indicating the small influence of the heating rate on thermal resistance. In the meantime,  $T_p$ ,  $DTG_p$  and  $DTG_m$  are all directly acquired from DTG curves for four heating rates, the  $CPI$  value is then estimated according to Equation (2), and the results are given in Table 1 as well. By comparing the  $CPI$  values, it may be plausibly deduced that a higher heating rate tends to demonstrate better thermochemical features. A similar finding on the heating-rate effect was also reported in our earlier work [39,40].

**Table 1.** Some featured parameters for pyrolysis of N-PE waste.

Parameters	$\beta$ (K/min)			
	5	10	15	20
$T_5$ (K)	658.43	675.94	685.10	690.82
$T_{30}$ (K)	685.38	701.12	714.17	719.59
$HRI$ (K)	330.55	338.61	344.25	346.96
$T_i$ (K)	600.61	602.75	601.72	597.74
$T_p$ (K)	701.46	719.14	735.32	748.46
$DTG_p$ ( $\text{min}^{-1}$ )	-0.113	-0.189	-0.264	-0.315
$DTG_m$ ( $\text{min}^{-1}$ )	-0.016	-0.030	-0.038	-0.051
$\Delta T$ (K)	51.97	62.81	57.04	68.90
$CPI$ ( $\times 10^{10} \text{ min}^{-2} \cdot \text{K}^{-3}$ )	0.82	2.07	4.02	5.27

Figure 4 shows the DTA results obtained over 5~20 K/min for the N-PE waste, where two endothermic melting valleys are observed for each heating rate due to the presence of two different crystalline structures. Obviously, they are, respectively, attributed to PE and

nylon-6 crystals with melting points corresponding to 396~400 K and 496~500 K. These melting point values are consistent with those in the literature [7,41,42]. Unsurprisingly, two valley temperatures are seen to strongly depend on the heating rate as reflected by the change in the melting temperatures with the heating rate, similar to that observed for the  $T_p$  value.

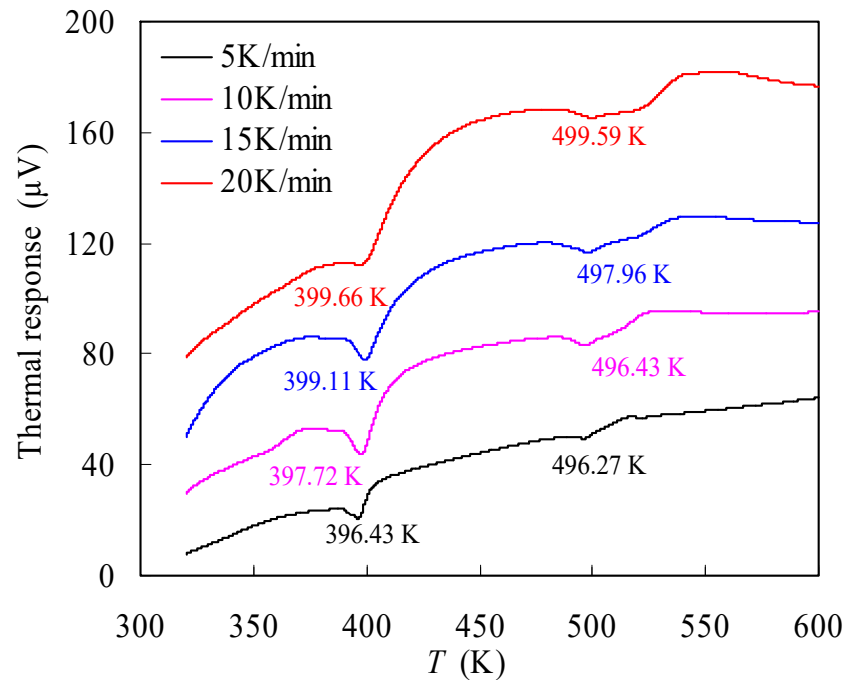


**Figure 4.** DTA results measured in  $N_2$  for N-PE waste.

### 3.3. Kinetics Analysis of Thermal Degradation

#### 3.3.1. Determination of $E_k$ with Various Kinetic Methods

Generally, the  $E_k$  can be readily computed via various model-free methods by linearly drawing an Arrhenius plot without the use of any assumed mechanism functions. After we collected the data ( $\alpha$ ,  $T$ ) from TG results over the range of  $0.01 \leq \alpha \leq 0.99$  for  $5 \leq \beta \leq 20$  K/min, the linear plots were drawn according to the four integral CR, FWO, MKN and SK methods. Figure S1 linearly presents the CR plots of  $\ln(\beta/T^2) \sim 1000/T$ , FWO plots of  $\ln(\beta) \sim 1000/T$ , MKN plots of  $\ln(\beta/T^{1.884318}) \sim 1000/T$  and SK plots of  $\ln(\beta/T^{1.92}) \sim 1000/T$  for the N-PE waste. As clearly seen, the plots exhibit very good linearity, and such finding can be also supported by the linear correlation coefficient  $R^2$  values because these values are mostly very close to 1.0 as shown in Figure 5. Estimated by using Equations (5)–(8) from the slopes of resultant straight lines, the  $E_k$  values are shown in Figure 5. In the meantime, the  $E_k$  can be iteratively obtained with the it-CR or it-FWO methods, and the  $E_k$  values thus achieved from the it-CR method are also given in Figure 5 along with the  $R^2$  values. It may be noted that the it-CR and it-FWO methods both led to identical results, and thus the results from the it-FWO method are not shown here.

As clearly seen, all the  $\alpha$ -dependent  $E_k$  curves show the same trend regardless of the model-free methods considered. However, the  $E_k$  values from CR, MKN, SK and more accurate iteration methods are very close to each other for all  $\alpha$  values, with a fluctuation of  $<0.5$  kJ/mol, but substantially lower than those from the FWO method. Overall, the  $E_k$  values from the FWO method are higher by 1.50~3.85 kJ/mol than those from the other methods. A careful examination shows that the  $E_k$  values are 143.41~213.72 kJ/mol for the CR method, 146.96~215.22 kJ/mol for the FWO method, 143.78~214.04 kJ/mol for the MKN method, 143.74~214.05 kJ/mol for the SK method and 143.79~214.05 kJ/mol for the it-CR/it-FWO method, respectively. If compared to those reported for individual nylon-6

pyrolysis [11–14] or PE pyrolysis [15–18], one may find their  $\alpha$ -dependent  $E_k$  values are almost the same, and for this reason, the  $E_k$  values for the co-pyrolysis of the N-PE waste are comparable to those of either nylon-6 or PE pyrolysis, indicative of the absence of the synergetic effect during the co-pyrolysis of the N-PE waste. After averaging, the  $E_k$  values for the five methods are 169.68, 172.66, 170.01, 170.03 and 170.04 kJ/mol, respectively.

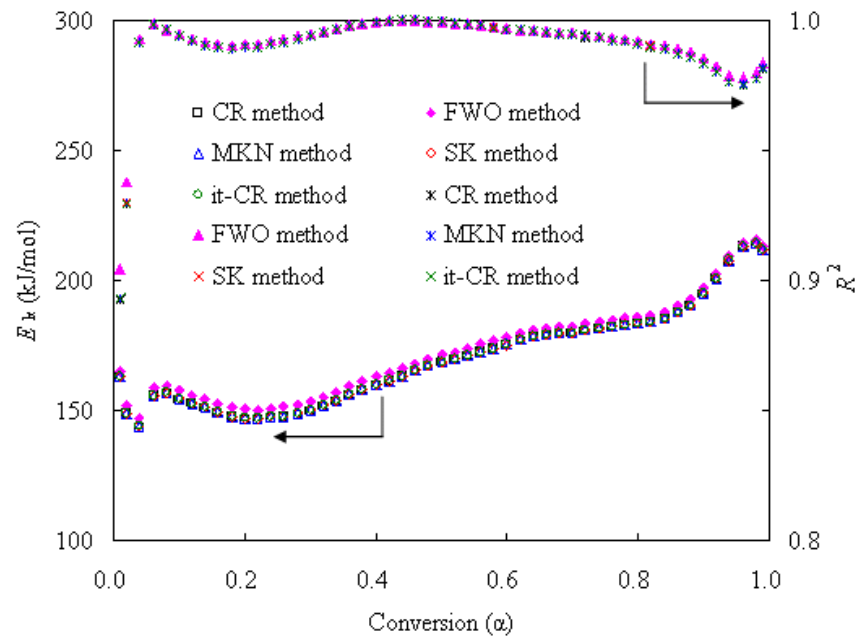


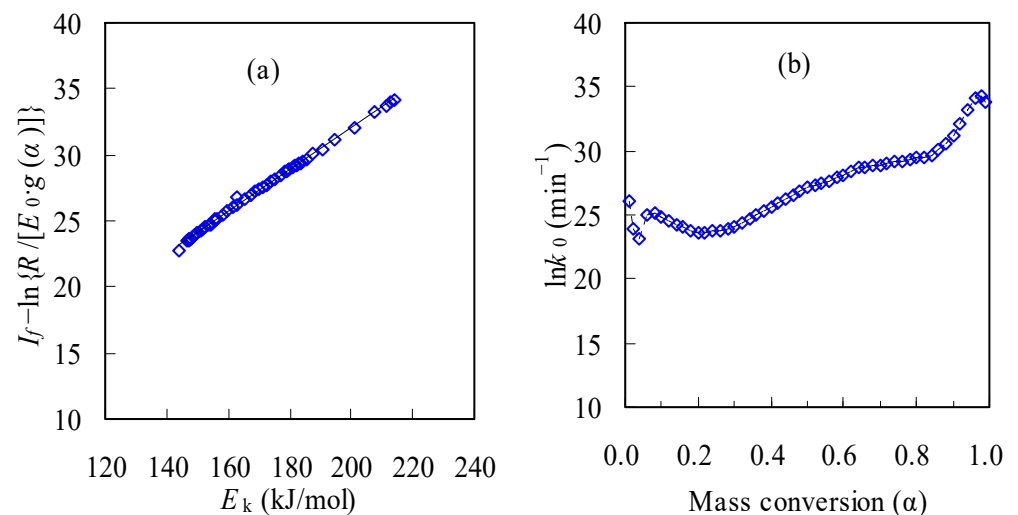
**Figure 5.**  $E_k$  calculated with various methods and calculation deviations  $R^2$  for pyrolysis of N-PE waste.

### 3.3.2. Determination of $g(\alpha)$ and $\ln k_0$ Based on Compensation Effect

Apart from  $E_k$ , the other two parameters  $\ln k_0$  and  $G(a)$  are determined by fully considering the compensation effect. It may be noted that one global reaction model is assumed here since there is only one peak in each DTG curve for the N-PE waste pyrolysis. Based on the it-CR method, the final intercepts of  $I_f$  are also achieved for all  $a$  values, and then a number of reaction model  $G(a)$  functions [19,20] are scanned with the aid of Equation (15). Subsequently, by linearly correlating the compensation effect, i.e.,  $I_f - \ln\{R/[E_k \cdot g(\alpha)]\}$  versus  $E_k$ , the correlation coefficient  $R^2$  can be yielded for examining the linearity of all the correlations, and the closer to 1.0 the  $R^2$  value is, the better the linear relationship. Therefore, among the reaction models considered, the one with the  $R^2$  closest to 1.0 will be taken as the most appropriate function for describing the pyrolysis of the N-PE sample. Table 2 shows the results for over 24 specific functions scanned for the compensation effect consideration [19,20]. Based on the results in Table 2, one may deduce that the co-pyrolysis of the N-PE waste appears to undergo a reaction-order-based chemical process or the Avrami–Erofeev nucleation mechanism. Furthermore, the  $A_{3/2}$  model function,  $g(\alpha) = [-\ln(1 - \alpha)]^{2/3}$ , seems to be the best one among the 24 specific pyrolysis mechanism models because it led to the closest  $R^2$  value of 0.9981, as shown in Table 2. Obviously, such a mechanism model is not like the chemical reaction mechanism model reported for the pyrolysis of nylon-6 [11–14] or PE [15–18], suggesting that the co-pyrolysis of the nylon-6/PE blend may have involved mutual interference from individual pyrolysis, leading to the change in the pyrolysis mechanism. With  $a$  and  $b$  thus obtained, the  $\ln k_0$  values are calculated by substituting the  $E_k$  values from the it-CR method into Equation (15) accordingly. These  $\ln k_0$  values are shown in Figure 6, along with the linear compensation effect from the  $A_{3/2}$  model. The  $\ln k_0$  values are seen to be  $a$ -dependent as well, like the  $E_k$  reflected in Figure 5. The  $\ln k_0$  is observed to vary from 23.14 to 34.26  $\text{min}^{-1}$  for the N-PE waste, and the  $k_0$  values are correspondingly in the range of  $1.12 \times 10^{10} \sim 7.56 \times 10^{14} \text{ min}^{-1}$ .

**Table 2.** Some specific function  $g(\alpha)$  scanned and calculation results.

No.	Symbol	$g(\alpha)$ Function	$\ln k_0 = a \cdot E_k + b$		$R^2$
			$a$	$b$	
Chemical reaction equation					
1	$F_{1/3}$	$g(\alpha) = 1 - (1 - \alpha)^{2/3}$	0.1631	-1.3526	0.9931
2	$F_{1/2}$	$g(\alpha) = 1 - (1 - \alpha)^{1/2}$	0.1660	-2.0653	0.9934
3	$F_{2/3}$	$g(\alpha) = 1 - (1 - \alpha)^{1/3}$	0.1693	-2.9472	0.9938
4	$F_{3/4}$	$g(\alpha) = 1 - (1 - \alpha)^{1/4}$	0.1710	-3.4938	0.9940
5	$F_{3/2}$	$g(\alpha) = (1 - \alpha)^{-1/2} - 1$	0.1909	-5.7914	0.9953
6	$F_2$	$g(\alpha) = (1 - \alpha)^{-1} - 1$	0.2080	-7.6834	0.9938
7	$F_3$	$g(\alpha) = (1 - \alpha)^{-2} - 1$	0.2477	-13.0338	0.9848
8	$F_1$	$g(\alpha) = -\ln(1 - \alpha)$	0.1768	-2.9720	0.9947
9	$G_1$	$g(\alpha) = 1 - (1 - \alpha)^2$	0.1481	1.8709	0.9932
10	$G_2$	$g(\alpha) = 1 - (1 - \alpha)^3$	0.1421	3.0684	0.9943
11	$G_3$	$g(\alpha) = 1 - (1 - \alpha)^4$	0.1381	3.8420	0.9951
Sigmoidal rate equation					
12	$A_{1/3}$	$g(\alpha) = [-\ln(1 - \alpha)]^3$	0.2879	-23.0267	0.9080
13	$A_{1/2}$	$g(\alpha) = [-\ln(1 - \alpha)]^2$	0.2323	-12.9993	0.9528
14	$A_{2/3}$	$g(\alpha) = [-\ln(1 - \alpha)]^{3/2}$	0.2046	-7.9856	0.9763
15	$A_{3/4}$	$g(\alpha) = [-\ln(1 - \alpha)]^{4/3}$	0.1953	-6.3144	0.9834
16	$A_{3/2}$	$g(\alpha) = [-\ln(1 - \alpha)]^{2/3}$	0.1583	0.3705	0.9981
17	$A_{5/2}$	$g(\alpha) = [-\ln(1 - \alpha)]^{2/5}$	0.1435	3.0445	0.9900
18	$A_2$	$g(\alpha) = [-\ln(1 - \alpha)]^{1/2}$	0.1491	2.0417	0.9946
19	$A_3$	$g(\alpha) = [-\ln(1 - \alpha)]^{1/3}$	0.1398	3.7129	0.9856
20	$A_4$	$g(\alpha) = [-\ln(1 - \alpha)]^{1/4}$	0.1352	4.5486	0.9785
Other mechanism equation					
21	$P_{1/2}$	$g(\alpha) = \alpha^{1/2}$	0.1398	3.4122	0.9914
22	$P_{1/3}$	$g(\alpha) = \alpha^{1/3}$	0.1336	4.6266	0.9821
23	$G_7$	$g(\alpha) = [1 - (1 - \alpha)^{1/2}]^{1/2}$	0.1437	2.4951	0.9929
24	$G_8$	$g(\alpha) = [1 - (1 - \alpha)^{1/3}]^{1/2}$	0.1453	2.0541	0.9935

**Figure 6.** Linear compensation plots (a) and resultant  $\ln k_0$  (b) for N-PE waste.

With fully available kinetic triplets, theoretical predications for the pyrolysis process were thus made, and Figure 7 exhibits the predicted results along with experimental data. As can be seen, the  $A_{3/2}$  mechanism model, combined with  $E_k$  from the iteration method and  $\ln k_0$  data from the compensation effect, excellently recast the  $\alpha \sim T$  curves over the entire range of 0.01~0.99 for the N-PE waste because the data points abstracted for each  $\beta$  are nearly all collapsed on their respective prediction curves.

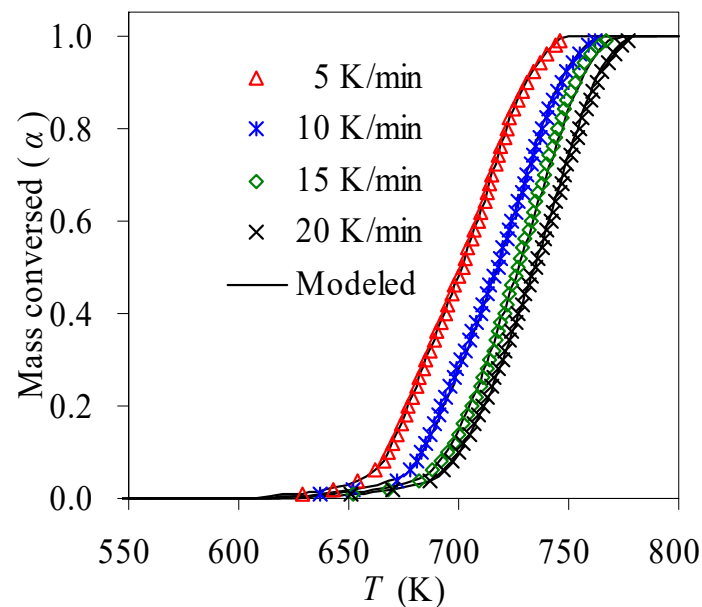


**Figure 7.** Predicated  $\alpha$ - $T$  curves and experimental results for N-PE waste.

### 3.3.3. Service Life Prediction

Lifetime information is very useful to properly consider a polymer for specific use requirements, and usually, the service time of various polymer-based products will be shortened under relatively high temperature conditions. Here, the lifespan of the N-PE waste was studied for thermal treatment consideration. Following the work earlier reported [31,43], it may be reasonably assumed that the plastic article cannot serve anymore when its mass loss approaches 5%, i.e.,  $\alpha = 0.05$ , and then the life span,  $t_s$ , can be estimated with the following expression:

$$t_s = \frac{g(\alpha)}{k_p} \exp\left(\frac{E_p}{RT}\right) \quad (21)$$

where  $E_p$  is the activation energy evaluated according to Kissinger's plot of  $\ln(\beta/T_p^2)$  versus  $1/T_p$ , and  $g(\alpha)$  is taken to follow the first-order reaction with  $g(\alpha) = -\ln(1 - \alpha)$  while  $k_p$  is the pre-exponential factor which is obtained as given below:

$$k_p = \frac{\beta E_p}{RT_p^2} \exp\left(\frac{E_p}{RT_p}\right) \quad (22)$$

Using the  $T_p$  data, Kissinger's plot can be drawn accordingly and is shown in Figure 8a. From the resultant line slope, the  $E_p$  thus calculated is 120.48 kJ/mol, and clearly, it is considerably smaller than those obtained with model-free methods. Subsequently, the  $\ln k_p$  value is estimated by using Equation (22) and varies very little with the change in the heating rate  $\beta$ . The  $\ln k_p$  averaged over four  $\beta$ s is  $18.79 \text{ min}^{-1}$ . Thereafter, the lifetime prediction can be performed with the use of  $E_p$  and  $\ln k_p$ , and the results are presented in Figure 8b.

As obviously seen,  $t_s$  is heavily relying on temperature, and it declines substantially with the rise in temperature. These findings agree with those reported in the literature [31,32]. According to the estimation, it may be noted that such packaging bags can withstand 100 °C very well for approximately 49.5 years, but the service time  $t_s$  at 150 °C will be reduced to about 0.5 years or 183 days. This information provides meaningful knowledge for selecting proper thermal conditions for applying polymer-based products.

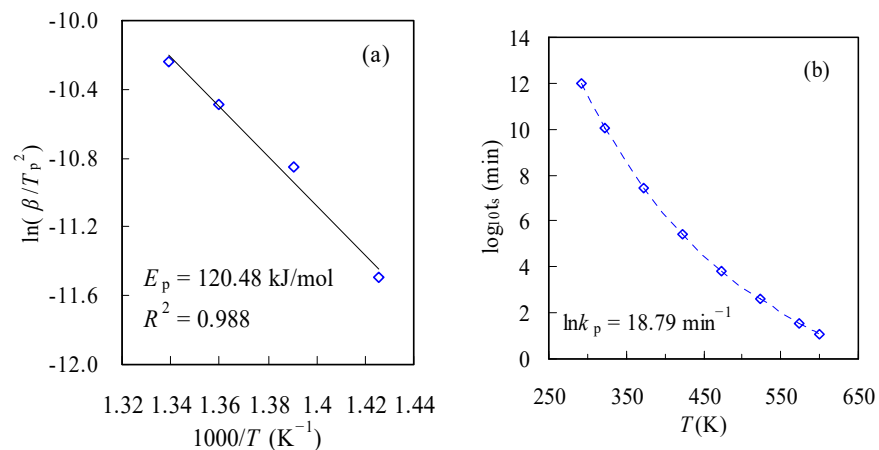


**Figure 8.** Kissinger's plot of  $\ln(\beta/T_p^2) \sim 1/T_p$  (a) and lifetime prediction (b) for N-PE waste.

### 3.3.4. Thermodynamic Parameters

Thermodynamic analysis may be performed for the pyrolysis of the N-PE waste according to the transition state theory [31–33]. Accordingly, thermodynamic quantities in terms of  $\Delta G$ ,  $\Delta H$  and  $\Delta S$ , i.e., the enthalpy change, entropy change and Gibbs free energy change, respectively, were calculated using the  $E_a$  values from the it-CR method and  $\ln k_0$  from the linear compensation effect. These parameters thus calculated are presented in Figure 9. As can be seen, all the  $\Delta H$  values are positive but  $\alpha$ -dependent over the whole conversion range, indicative of an endothermic feature. Thus, external energy must be provided for conducting the waste pyrolysis. In contrast, the  $\Delta G$  values almost remain unchangeable around 187.66 kJ/mol over  $0.01 < \alpha < 0.99$ . These positive  $\Delta G$  values suggest a thermodynamically non-spontaneous process that requires the heat introduced for undergoing pyrolysis. Furthermore, as mass conversion progresses, the proceeding pyrolysis becomes less favorable as reflected by higher  $\Delta G$  for higher  $\alpha$  values. As also observed from Figure 9, most  $\Delta S$  values, ranging from  $-66.66$  to  $23.83$  J/mol·K, are negative during the pyrolysis process, indicating a transition from a disordered state to an ordered state according to the transition state theory. However, such ordering is rather dubious since high-molecular-weight polymers will crack into small molecules during high-temperature pyrolysis. Further work along this line is thus required and should be conducted to deeply understand the thermodynamics of pyrolysis.

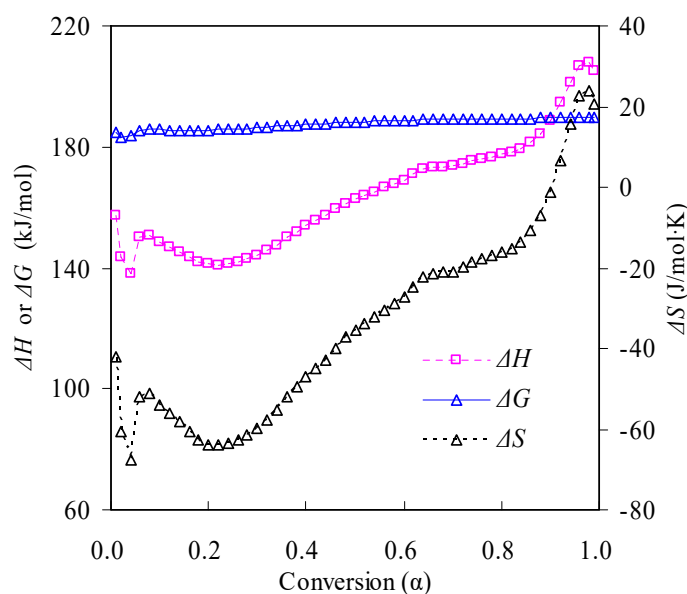


**Figure 9.** Thermodynamic parameters  $\Delta H$ ,  $\Delta S$  and  $\Delta G$  for the N-PE waste pyrolysis.

#### 4. Conclusions

In this work, the pyrolysis of N-PE pouch waste was studied non-isothermally under 5–20 K/min, and kinetic and thermodynamic analyses were thus conducted in detail. Some conclusions may be drawn as follows:

1. TGA results show that the co-pyrolysis of the N-PE pouch waste underwent one decomposition stage, indicating that the respective pyrolyses of nylon-6 and PE may overlap with each other. In the meantime, all specific temperatures of  $T_1$ ,  $T_5$ ,  $T_{30}$ ,  $T_p$  and  $T_{99}$  and pyrolysis performance parameters  $CPI$  and  $HRI$  are all found to increase with the heating rate.
2. The co-pyrolysis of the N-PE pouch waste was kinetically analyzed, and the  $E_k$  values from the isoconversional CR, MKN, SK, it-CR and it-FWO methods are very similar to each other, whereas the ones from the FWO method are fairly higher. For all these methods, the  $E_k$  values within 143–215 kJ/mol demonstrated strictly the same  $\alpha$ -dependence.
3. The methodology of combining model fitting with the compensation effect was tried for seeking the pyrolysis mechanism together with the pre-exponential factor, resulting in the  $A_{3/2}$  model of  $g(\alpha) = [-\ln(1 - \alpha)]^{2/3}$ , or  $f(\alpha) = 3/2 (1 - \alpha) \cdot [-\ln(1 - \alpha)]^{1/3}$  with the  $k_0$  range of  $1.12 \times 10^{10} \sim 7.56 \times 10^{14} \text{ min}^{-1}$  for the pyrolysis of the N-PE waste. With  $E_k$ ,  $k_0$  and  $g(\alpha)$  thus obtained, the  $\alpha$ -T curves were calculated and then demonstrated very satisfactory correlations against experimental results.
4. Thermodynamic parameters in terms of  $\Delta G$ ,  $\Delta H$  and  $\Delta S$  and the service lifetime predictions were estimated concerning the pyrolysis decomposition process of the N-PE waste, and the information provided helpful knowledge for applying polymer-based products and future waste disposal.

**Supplementary Materials:** The following supporting information can be downloaded at: <https://www.mdpi.com/article/10.3390/ma16175738/s1>, Figure S1: The Arrhenius linear plots of the N-PE waste with: (a) CR method, (b) FWO method, (c) MKN method and (d) SK method.

**Author Contributions:** Conceptualization, H.-B.W. and Z.H.; Methodology, H.-B.W.; Validation, Z.H.; Formal analysis, Z.H.; Investigation, H.-B.W.; Data curation, Z.H.; Writing—original draft, H.-B.W.; Writing—review and editing, Z.H.; Supervision, Z.H. All authors contributed to the conceptualization and development of the manuscript. H.-B.W. conducted sample collection and preparation, ran experiments, performed data analysis and prepared the first draft. Z.H. contributed to the experiment design, data analysis, manuscript writing and finalization of the manuscript. All authors have read and agreed to the published version of the manuscript.

**Funding:** Not applicable.

**Institutional Review Board Statement:** Not applicable.

**Informed Consent Statement:** Not applicable.

**Data Availability Statement:** The data presented in this study are available on request from the corresponding author.

**Conflicts of Interest:** We declare that there is not any conflict of interest related to the above-mentioned work.

#### References

1. Bugatti, V.; Zuppari, F.; Viscusi, G.; Gorrasi, G. Active packaging based on coupled nylon/PE pouches filled with active nano-hybrid: Effect on the shelf life of fresh milk. *Nanomaterials* **2021**, *11*, 1881. [[CrossRef](#)] [[PubMed](#)]
2. Kang, J.H.; Jeon, Y.J.; Min, S.C. Effects of packaging parameters on the microbial decontamination of Korean steamed rice cakes using in-package atmospheric cold plasma treatment. *Food Sci. Biotechnol.* **2021**, *30*, 1535–1542. [[CrossRef](#)] [[PubMed](#)]
3. Mangaraj, S.; Goswami, T.K.; Mahajan, P.V. Applications of plastic films for modified atmosphere packaging of fruits and vegetables: A review. *Food Eng. Rev.* **2009**, *1*, 133–158. [[CrossRef](#)]
4. Harmon, R.E.; SriBala, G.; Broadbelt, L.J.; Burnham, A.K. Insight into polyethylene and polypropylene pyrolysis: Global and mechanistic models. *Energy Fuels* **2021**, *35*, 6765–6775. [[CrossRef](#)]

5. Xu, F.F.; Wang, B.; Yang, D.; Hao, J.H.; Qiao, Y.Y.; Tian, Y.Y. Thermal degradation of typical plastics under high heating rate conditions by TG-FTIR: Pyrolysis behaviors and kinetic analysis. *Energy Convers. Manag.* **2018**, *171*, 1106–1115. [[CrossRef](#)]
6. Dubdub, I.; Al-Yaari, M. Thermal behavior of mixed plastics at different heating rates: I. Pyrolysis kinetics. *Polymers* **2021**, *13*, 3413. [[CrossRef](#)]
7. Budrugaec, P.; Cucos, A.; Dascălu, R.; Atkinson, I.; Osiceanu, P. Application of model-free and multivariate nonlinear regression methods for evaluation of the kinetic scheme and kinetic parameters of thermal decomposition of low density polyethylene. *Thermochim. Acta* **2022**, *708*, 179138. [[CrossRef](#)]
8. Koga, N.; Vyazovkin, S.; Burnham, A.K.; Favergeon, L.; Muravyev, N.V.; Perez-Maqueda, L.A.; Saggese, C.; Sánchez-Jiménez, P.E. ICTAC Kinetics Committee recommendations for analysis of thermal decomposition kinetics. *Thermochim. Acta* **2023**, *719*, 179384. [[CrossRef](#)]
9. Vyazovkin, S.; Burnham, A.K.; Favergeon, L.; Koga, N.; Moukhina, E.; Pérez-Maqueda, L.A.; Sbirrazzuoli, N. ICTAC Kinetics Committee recommendations for analysis of multi-step kinetics. *Thermochim. Acta* **2022**, *689*, 178597. [[CrossRef](#)]
10. Muravyev, N.V.; Vyazovkin, S. The status of pyrolysis kinetics studies by thermal analysis: Quality is not as good as it should and can readily be. *Thermo* **2022**, *2*, 435–452. [[CrossRef](#)]
11. Kim, S.S.; Jeon, J.K.; Park, Y.K.; Kim, S. Thermal pyrolysis of fresh and waste fishing nets. *Waste Manag.* **2005**, *25*, 811–817. [[CrossRef](#)] [[PubMed](#)]
12. Eimontas, J.; Yousef, S.; Striūgas, N.; Abdelnaby, M.A. Catalytic pyrolysis kinetic behaviour and TG-FTIR-GC-MS analysis of waste fishing nets over ZSM-5 zeolite catalyst for caprolactam recovery. *Renew. Energy* **2021**, *179*, 1385–1403. [[CrossRef](#)]
13. Pannase, A.M.; Singh, R.K.; Ruj, B.; Gupta, P. Decomposition of polyamide via slow pyrolysis: Effect of heating rate and operating temperature on product yield and composition. *J. Anal. Appl. Pyrolysis* **2020**, *151*, 104886. [[CrossRef](#)]
14. Bockhorn, H.; Donner, S.; Gernsbeck, M.; Hornung, A.; Hornung, U. Pyrolysis of polyamide 6 under catalytic conditions and its application to reutilization of carpets. *J. Anal. Appl. Pyrolysis* **2001**, *58–59*, 79–94. [[CrossRef](#)]
15. Sinfrônio, F.S.M.; Santos, J.C.O.; Pereira, L.G.; Souza, A.G.; Conceição, M.M.; Fernandes, V.J., Jr.; Fonseca, V.M. Kinetic of thermal degradation of low-density and high-density polyethylene by non-isothermal thermogravimetry. *J. Thermal Anal. Calorim.* **2005**, *79*, 393–399. [[CrossRef](#)]
16. Encinar, J.M.; González, J.F. Pyrolysis of synthetic polymers and plastic wastes. *Fuel Process. Technol.* **2008**, *89*, 678–687. [[CrossRef](#)]
17. Aboulkas, A.; El Harfi, K.; El Bouadili, A. Thermal degradation behaviours of polyethylene and propylene. Part I: Pyrolysis and mechanism. *Energy Convers. Manag.* **2010**, *51*, 1363–1369. [[CrossRef](#)]
18. Wang, Z.; Wei, R.; Ning, X.; Xie, T.; Wang, J. Thermal degradation properties of LDPE insulation for new and aged fine wires. *J. Thermal Anal. Calorim.* **2019**, *137*, 461–471. [[CrossRef](#)]
19. Chen, R.Y.; Li, Q.W.; Xu, X.K.; Zhang, D.D. Pyrolysis kinetics and reaction mechanism of representative non-charring polymer waste with micron particle size. *Energy Convers. Manag.* **2019**, *198*, 111923. [[CrossRef](#)]
20. Trache, D.; Abdelaziz, A.; Siouani, B. A simple and linear isoconversional method to determine the pre-exponential factors and the mathematical reaction mechanism functions. *J. Thermal Anal. Calorim.* **2017**, *128*, 335–348. [[CrossRef](#)]
21. Sygula, E.; Swiechowski, K.; Hejna, M.; Kunaszyk, I.; Białowiec, A. Municipal solid waste thermal analysis-Pyrolysis kinetics and decomposition reactions. *Energies* **2021**, *14*, 4510. [[CrossRef](#)]
22. Komandur, J.; Kumar, A.; Para, P.; Mohanty, K. Kinetic parameters estimation of thermal and co-pyrolysis of groundnut de-oiled cake and polyethylene terephthalate (PET) waste. *Energies* **2022**, *15*, 7502. [[CrossRef](#)]
23. Coats, A.W.; Redfern, J.P. Kinetic parameters from thermogravimetric data. *Nature* **1964**, *201*, 68–69. [[CrossRef](#)]
24. Ozawa, T. A new method of analyzing thermogravimetric data. *Bull. Chem. Soc. Jpn.* **1965**, *38*, 1881–1886. [[CrossRef](#)]
25. Flynn, J.H.; Wall, L.A. General treatment of thermogravimetry of polymers. *J. Res. Natl. Bur. Stand. Sect. A Phys. Chem.* **1966**, *70A*, 487–523. [[CrossRef](#)]
26. Madhysudanan, P.M.; Krishnan, K.; Ninan, K.N. New equations for kinetic analysis of non-isothermal reactions. *Thermochim. Acta* **1993**, *221*, 13–21. [[CrossRef](#)]
27. Starink, M.J. The determination of activation energy from linear heating rate experiments: A comparison of the accuracy of isoconversion methods. *Thermochim. Acta* **2003**, *404*, 163–176. [[CrossRef](#)]
28. Akahira, T.; Sunose, T. Method of determining activation deterioration constant of electrical insulating materials. *Res. Rep. Chiba Inst. Technol.* **1971**, *16*, 22–31.
29. Gao, Z.M.; Nakada, M.; Amasaki, I. A consideration of errors and accuracy in the isoconversional methods. *Thermochim. Acta* **2001**, *369*, 137–142. [[CrossRef](#)]
30. Vyazovkin, S. Determining pre-exponential factor in model-free kinetic methods: How and why? *Molecules* **2021**, *26*, 3077. [[CrossRef](#)]
31. Georgieva, V.; Zvedova, D.; Vlaev, L. Non-isothermal kinetics of thermal degradation of chitin. *J. Thermal Anal. Calorim.* **2013**, *111*, 763–771. [[CrossRef](#)]
32. Hao, Y.H.; Huang, Z.; Ye, Q.Q.; Wang, J.W.; Yang, X.Y.; Fan, X.Y.; Li, Y.L.; Peng, Y.W. A comparison study on non-isothermal decomposition kinetics of chitosan with different analysis methods. *J. Thermal Anal. Calorim.* **2017**, *128*, 1077–1091. [[CrossRef](#)]
33. Wan, H.B.; Huang, Z. Pyrolysis and oxidative thermal decomposition investigations of tennis ball rubber wastes through kinetic and thermodynamic evaluations. *Materials* **2023**, *16*, 2328. [[CrossRef](#)] [[PubMed](#)]

34. Porubská, M.; Szöllös, O.; Kóňová, A.; Janigová, I.; Jašková, M.; Jomová, K.; Chodák, I. FTIR spectroscopy study of polyamide-6 irradiated by electron and proton beams. *Polym. Degrad. Stab.* **2012**, *97*, 523–531. [[CrossRef](#)]
35. Duque, J.V.F.; Martins, M.F.; Bittencourt, F.L.F.; Debenest, G.; Orlando, M.T.D.; Profeti, L.P.R.; Profeti, D. Recovering wax from polyethylene waste using C-DPyR. *Energy* **2023**, *272*, 127135. [[CrossRef](#)]
36. Jaiswal, P.B.; Pushkar, B.K.; Maikap, K.; Mahanwar, P.A. Abiotic aging assisted bio-oxidation and degradation of LLDPE/LDPE packaging polyethylene film by stimulated enrichment culture. *Polym. Degrad. Stab.* **2022**, *206*, 110156. [[CrossRef](#)]
37. Gu, J.W.; Yang, X.T.; Li, C.M.; Kou, K.C. Synthesis of cyanate ester microcapsules via solvent evaporation technique and its application in epoxy resins as a healing agent. *Ind. Eng. Chem. Res.* **2016**, *55*, 10941–10946. [[CrossRef](#)]
38. Fang, S.W.; Yu, Z.S.; Lin, Y.S.; Hu, S.C.; Liao, Y.F.; Ma, X.Q. Thermogravimetric analysis of the co-pyrolysis of paper sludge and municipal solid waste. *Energy Convers. Manag.* **2015**, *101*, 626–631. [[CrossRef](#)]
39. Wan, H.B.; Huang, Z. Pyrolysis evaluation of tennis string polyurethane and water-borne polyurethane wastes through isoconversional kinetic analysis. *Polymers* **2022**, *14*, 1501. [[CrossRef](#)]
40. Wan, H.B.; Huang, Z. Kinetic analysis of pyrolysis and thermo-oxidative decomposition of tennis string nylon wastes. *Materials* **2021**, *14*, 7564. [[CrossRef](#)]
41. Yu, J.C.; Gröbner, G.; Tonpheng, B.; Andersson, O. Microstructure, nucleation and thermal properties of high-pressure crystallized MWCNT/nylon-6 composites. *Polymer* **2011**, *52*, 5521–5527. [[CrossRef](#)]
42. Bateni, F.; Motlagh, G.H. Electrospun polyamide/graphene oxide nanofibers as fillers for polyethylene: Preparation and characterization. *J. Appl. Polym. Sci.* **2021**, e51506. [[CrossRef](#)]
43. Vyazovkin, S.; Burnham, A.K.; Criado, J.M.; Pérez-Maqueda, L.A.; Popescu, C.; Sbirrazzuoli, N. ICTAC Kinetics Committee recommendations for performing kinetic computations on thermal analysis data. *Thermochim. Acta* **2011**, *520*, 1–19. [[CrossRef](#)]

**Disclaimer/Publisher's Note:** The statements, opinions and data contained in all publications are solely those of the individual author(s) and contributor(s) and not of MDPI and/or the editor(s). MDPI and/or the editor(s) disclaim responsibility for any injury to people or property resulting from any ideas, methods, instructions or products referred to in the content.